Characterization of Diffuse Scattering in Yttria-Stabilized Zirconia by Electron Diffraction and High-Resolution Transmission Electron Microscopy

Susana García-Martín,*,† Duncan P. Fagg,‡ and John T.S. Irvine§

Departamento de Química Inorgánica, Facultad de Ciencias Químicas, Universidad Complutense, Madrid 28040, Spain, Nanotechnology Research Division, Centre of Mechanical Technology and Automation, University of Aveiro, 3810 193 Aveiro, Portugal, and School of Chemistry, University of St. Andrews, St. Andrews, Fife KY16 9ST, United Kingdom

Received July 4, 2008

Different phases from the $ZrO_2-Y_2O_3$ system corresponding to 8, 10, 14, 21, 32, and 37 mol % Y_2O_3, prepared by quenching from high temperature, have been studied by selected area electron diffraction (SAED) and high-resolution electron microscopy (HRTEM). The results of the 8 and 10 mol% Y_2O_3 are consistent with a crystal microstructure of three kind of domains of the t or t′ phase with the *c* axes oriented along three mutually perpendicular directions and small displacements of the cations (Zr and Y) from their ideal crystallographic positions. The materials with higher dopant concentration show a modulated fluorite-type structure due to partial or short-range ordering of the oxygen vacancies related to a pyrochlore-type and/or C-type crystal structures.

Introduction

The highest-temperature polymorph of the ZrO_2 is a cubic phase with fluorite-type structure, which can be stabilized to room temperature by the addition of lower valence oxides and quenching from appropriate high temperatures leading to anion deficient materials called stabilized zirconias. Among this type of materials, yttria-stabilized zirconias (YSZs) are probably the most studied because of their important technological applications derived from their physical properties.

Modifications of the equilibrium phase diagram of the $ZrO_2-Y_2O_3$ system firstly reported by Scott[1] have been proposed by other researchers,[2] mainly in the position of the phase boundaries of the zirconia-rich region (around 1000 °C). The origin of the discrepancies may be due to different methods used for preparing samples and different thermal treatments throughout the studies or incomplete quenching of the samples from high temperature. However, the highest-temperature metastable phases are the most interesting from the point of view of their properties and commercial applications, in particular those with 0−10 mol % Y_2O_3.

In this sense, the high oxygen ion mobility of the YSZ's allows them to be used as solid electrolytes in solid oxide fuel cells. The highest conductivity occurs in the cubic phase with an yttria content of about 8 mol %.[3,4] Higher dopant concentrations produce a decrease in ionic conductivity and an increase in activation energy, which is thought to arise from some kind of anion-vacancy association, reducing the number of free oxygen vacancies available for oxygen transport. However, the nature of the defect association, the existence of anion vacancy and/or cation ordering, the nature of the interaction between the dopant cation and zirconium ions with vacancies (i.e., the crystal microstructure of the YSZ's) is still an open question, despite the enormous amount of work, using a great variety of experimental techniques, found in the literature dedicated to this aspect.

The phase diagrams of the $ZrO_2-Y_2O_3$ system have usually been established from conventional powder X-ray diffraction results, which give information on the average crystal structure; local or short-range effects cannot be detected by this technique. The phase diagrams all indicate that the cubic phase is stable from 8 mol % Y_2O_3 at high temperatures. On the contrary, even in high temperature quenched phases of the cubic region of the phase diagram, in addition to the Bragg reflections characteristic of the fluorite structure, weak superlattice reflections, and/or diffuse diffraction are observed by electron diffraction,[5−7] single-crystal X-ray diffraction.[8−10] and neutron diffraction[11−13]

* Corresponding author. E-mail: sgmartin@quim.ucm.es.
† Universidad Complutense.
‡ University of Aveiro.
§ University of St. Andrews.

(1) Scott, H. G. *J. Mater. Sci.* **1975**, 10.
(2) Yashima, M.; Kakihana, M.; Yoshimura, M. *Solid State Ionics* **1996**, *1131*, 86–88, and references therein.
(3) Badwal, S. P. S. *J. Mater. Sci.* **1985**, *20*, 4593.
(4) Badwal, S. P. S. *Solid State Ionics* **1992**, *52*, 23.
(5) Lanteri, V.; Chaim, R.; Heuer, A. H. *J. Am. Ceram. Soc.* **1986**, *69* (10), C-258.
(6) Zhou, Y.; Lei, T. C.; Sakuma, T. *J. Am. Ceram. Soc.* **1991**, *74* (3), 633.
(7) Butz, B.; Kruse, P.; Störmer, H.; Gerthsen, D.; Müller, A.; Weber, A.; Ivers-Tiffée, E. *Solid State Ionics* **2006**, *177*, 3275.
(8) Welberry, T. R.; Withers, R. L.; Thompson, J. G.; Butler, B. D. *J. Solid State Chem.* **1992**, *100*, 71.
(9) Welberry, T. R.; Butler, B. D.; Thompson, J. G.; Withers, R. L. *J. Solid State Chem.* **1993**, *106*, 461.
(10) Welberry, T. R.; Withers, R. L.; Mayo, S. C. J. *Solid State Chem.* **1995**, *115*, 43.
(11) Hull, S.; Farley, T. W.D.; Hackett, M. A.; Hayes, W.; Osborn, R.; Andersen, N. H.; Clausen, K.; Hutchings, M. T.; Stirling, W. G. *Solid State Ionics* **1988**, *488*, 28–30.

10.1021/cm801818y CCC: $40.75
Published on Web 08/27/2008

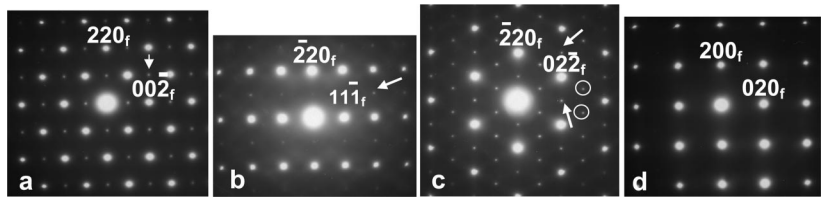

Figure 1. SAED patterns of 8YSZ along the (a) $[\bar{1}10]$, (b) $[\bar{1}1\bar{2}]$, (c) $[\bar{1}1\bar{1}]$, and (d) [001] zone axes.

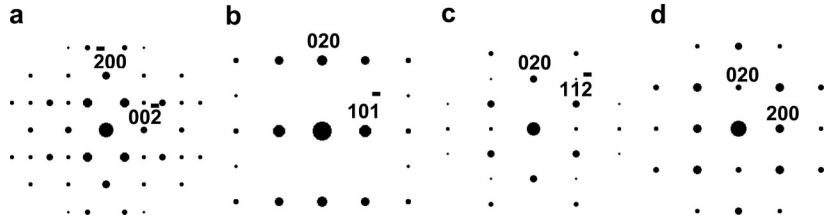

Figure 2. Calculated SAED patterns of t-ZrO_2 along the (a) $[0\bar{1}0]_f$, (b) $[\bar{1}0\bar{1}]_f$, (c) $[\bar{2}0\bar{1}]_f$, and (d) $[001]_f$ zone axes.

The superlattice reflections have generally been associated with different distortions of the cubic phase and the diffuse scattering to partial or short-range ordering of the anion vacancies, and/or to atomic displacements from their ideal crystallographic positions.

Here, we present a study of some phases from the $ZrO_2-Y_2O_3$ system prepared by quenching from high temperature by selected area electron diffraction (SAED) and high resolution electron microscopy (HRTEM). The aim of the work is to provide more detailed information of the crystal short range structure of stabilized zirconias with the purpose of contributing to the general understanding of their physical properties in relation to their crystal structure. We suggest new models for the crystal microstructure of the oxides of this system. These models not only offer an insight into the conduction behaviour of these materials but also provide appropriate arguments to discard some models previously presented in the literature.

Experimental Section

Different compositions in the $ZrO_2-Y_2O_3$ system corresponding to 8, 10, 14, 21, 32, and 37 mol % Y_2O_3 (i.e., $Zr_{0.85}Y_{0.15}O_{1.926}$ or 8YSZ, $Zr_{0.82}Y_{0.18}O_{1.91}$ or 10YSZ, $Zr_{0.75}Y_{0.25}O_{1.88}$ or 14YSZ, $Zr_{0.65}Y_{0.35}O_{1.825}$ or 21YSZ, $Zr_{0.5}Y_{0.5}O_{1.75}$ or 32YSZ, and $Zr_{0.46}Y_{0.54}O_{1.73}$ or 37YSZ,respectively) were prepared from stoichiometric amounts of ZrO_2 and Y_2O_3 ground under acetone using an agate pestle and mortar and dry pressed into pellets under a pressure of 3 tonnes/cm^2. Prior to weighing, it was necessary to dry Y_2O_3 for 24 h at 1000 °C to remove moisture and absorbed gases; ZrO_2 powder was dried at 700°C for 24 h. Samples were fired in air at 1450−1500°C for periods of 48−72 hours with intermediate grinding and repressing until single phase fluorite was achieved. Samples were rapidly cooled by removing from the furnace in alumina crucibles, which because of the refractory nature of these oxides effectively quenched their high-temperature structure to ambient.

Crystalline phase identification and determination of the lattice parameters were carried out by powder X-ray diffraction using a Stoe Stadi-P diffractometer with a position sensitive detector (PSD), Ge monochromator, and Cu−$K_{\alpha 1}$ radiation.

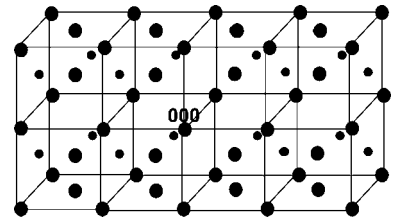

Figure 3. Drawing of the reciprocal lattice of three domains of t-ZrO_2 with common origin and *c* axes oriented along three mutually perpendicular directions.

For transmission electron microscopy, the samples were ground in *n*-butyl alcohol and ultrasonically dispersed. A few drops of the resulting suspension were deposited on a carbon-coated grid. SAED studies were performed with an electron microscope JEOL 2000FX (double tilt ±45°) working at 200 kV and HRTEM studies with an electron microscope JEOL 3000EX (double tilt ±20°) working at 300 kV.

Image calculations were performed using the MacTempas program based on the multislice approach.

Results and Discussion

Powder X-ray diffraction patterns of all the materials in this study indicate pure phases with a "defect fluorite" type cubic crystal structure (there is apparently neither cation nor anion vacancy ordering) in agreement with most of the phase diagrams proposed in the literature.[1]

Figure 1 shows four SAED patterns of 8YSZ along different zone axes. The patterns have been indexed according to the fluorite-type cell (f refers to the cubic fluorite structure). In addition to the Bragg reflections characteristic of the fluorite-type unit cell, superlattice reflections are observed at several positions in reciprocal space, which are not consistent with the reflection conditions of the space group of the fluorite structure ($Fm3m$: hhl $h + l = 2$; $0kl$ k, $l = 2n$; and hkl $h + k$, $h + l$, $k + l = 2n$). Reflections at $G_F \pm (11\bar{2})^*$ and $G_F \pm (13\bar{2})^*$ (indicated by arrows in the patterns) are characteristic of the tetragonal polymorph of the ZrO_2 (t and t′ phases) as shown in the calculated SAED

(12) Gibson, I. R.; Irvine, J. T. S. *J. Mater. Chem.* **1996**, *6*, 895.
(13) Goff, J. P.; Hayes, W.; Hull, S.; Hutchings, M. T.; Clausen, K. N. *Phys. Rev. B* **1999**, *59* (22), 14202.

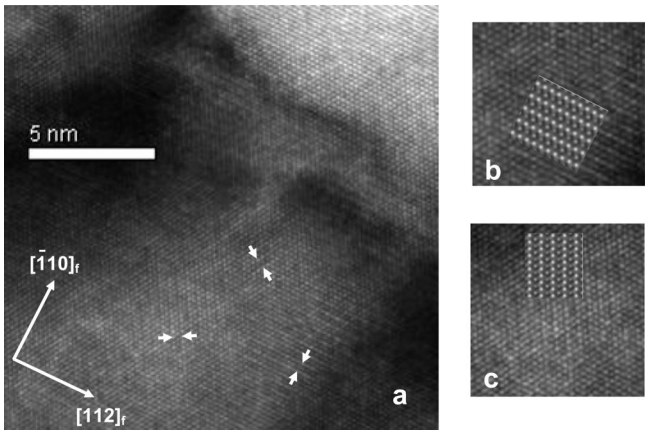

Figure 4. (a) HRTEM image of 8YSZ corresponding to the $[\bar{1}1\bar{1}]_f$ zone axis; (b, c) calculated images for cubic 8YSZ with 0.1 Å of cation displacements along the $[101]_f$ and $[011]_f$ directions, respectively, inserted in the experimental image.

patterns of this phase (Figure 2). However, there are still reflections in our patterns forbidden in this tetragonal phase, such as those at $G_F \pm (110)^*$, $G_F \pm (001)^*$ and $G_F \pm (02\bar{1})^*$.

Similar SAED patterns have been found for samples with composition 8,[6,7,14−17] 10,[7,15,16,18−20] and 12 mol % Y_2O_3[5,20] rapidly cooled from high temperatures. Zhou et al.[6] suggest that the appearance of reflections at $G_F \pm (112)^*$ is caused by small displacements of the oxygen ions from their ideal positions along the $[001]_f$, $[100]_f$, and $[010]_f$ directions, but the symmetry of the phase remains cubic (they name it c′ phase). McClellan et al.[19] propose a distortion of the oxygen sublattice from the ideal fluorite structure by displacement along the $[111]_f$ directions, giving also a cubic symmetry. Rao et al.[14] indicate the formation of $Y_{0.25}Zr_{0.75}O_{2-x}$ ($L1_2$) and $Y_{0.5}Zr_{0.5}O_{2-y}$ ($L1_0$) cation-ordered structures, in some regions of the crystals due to yttrium segregation, which originate the superlattice reflections at $G_F \pm (001)^*$ and $G_F \pm (110)^*$, but Kondoh et al. have related these extra reflections to some kind of periodic and anisotropic lattice distortions.[15,16] Other authors have explained their results on the basis of the diffusionless cubic to metastable tetragonal phase (t′) transformation accompanied by the formation of three t′ variants with the $c_{t'}$ axis being parallel to each of the three original $[001]_f$ directions.[5,17,18] Butz et al. have recently suggested the formation of tetragonal and monoclinic (m′) regions within the cubic grains of 8YSZ.[7]

Our SAED patterns of 8YSZ are consistent with a crystal microstructure of three kinds of domains of the t or t′ phase with the *c* axes oriented along three mutually perpendicular directions. Figure 3 shows the reciprocal lattice of these three domains with common origin. The domain formation is well-identified in the SAED pattern of the $[\bar{1}1\bar{1}]_f$ zone axis (Figure 1c): in addition to the reflections characteristic of the fluorite structure, there are superlattice reflections at $G_F \pm (11\bar{2})^*$ and $G_F \pm (\bar{1}3\bar{2})^*$ consistent with the tetragonal phase and at $G_F \pm (12\bar{3})^*$ and $G_F \pm (21\bar{3})^*$ (surrounded by white circles) also due to tetragonal phases but with different orientations of the unit cell. Besides, reflections at $G_F \pm (110)^*$, $G_F \pm (001)^*$, and $G_F \pm (021)^*$ arise by a double diffraction effect, the $G_F \pm (11\bar{2})^*$ position in reciprocal space being the origin of the secondary diffraction in the patterns of the $[\bar{1}10]_f$ and $[\bar{1}1\bar{1}]_f$ zone axes (patterns a and c in Figure 1) and the $G_F \pm (13\bar{2})^*$ position in the pattern along the $[\bar{1}1\bar{2}]_f$ zone axis.

However, the HRTEM images of this 8YSZ phase reveals peculiar contrast differences: Figure 4a shows the HRTEM image of the $[\bar{1}1\bar{1}]_f$ zone axis, which is characteristic of an average fluorite structure. Moreover, bright lattice fringes perpendicular to the $[\bar{1}10]_f$, $[\bar{1}01]_f$, and $[01\bar{1}]_f$ directions are observed in the thick areas of the crystal (indicated by arrows in the image), but distance between them ($\sim$3.6 Å $\approx d(110)_f$) does not imply a superperiodicity of the fluorite structure. We have performed image simulations as an aid to interpretation of the HRTEM images. The crystal structure models used for the image calculations are based on small displacements of the cations (Zr and Y) from their ideal crystallographic positions along different directions of the cubic or tetragonal phase of the fluorite type structure. Image simulation results are similar for ZrO_2 and ZrO_2 8 mo l% Y_2O_3. Images b and c in Figure 4 show two magnified areas of Figure 4a with calculated images of 8YSZ for 100 Å specimen thickness and 200 Å defocus of the objective lens inserted for comparison. The crystal structure model for the simulations corresponds to a cubic phase with 0.1 Å of cation displacements along the $[101]_f$ direction (along $[011]_f$ for the simulated image in Figure 4c). The calculated images show contrast differences to similar the experimental ones.

However, indistinguishable calculated images are obtained by displacing the cations along the $[100]_f$ or $[111]_f$ directions or using a tetragonal unit cell with cation displacements along [111] and [201] directions. Calculated SAED patterns of this crystal structure model consisting of cation displacements in the average fluorite structure (Figure 5) are consistent with the experimental patterns shown in Figure 1 (notice that only one domain has been taken into account for the calculation).

Cation displacements from the ideal fluorite sites have previously been reported in several YSZs: Ishizawa et al. studied ZrO_2 14 mol % Y_2O_3 by single-crystal X-ray diffraction, indicating that Zr atoms are displaced around 0.19 Å from the origin of the space group $F_m\bar{3}_m$ along $[111]_f$ while Y atoms remain at the origin.[21] Studies on ZrO_2 18 mol % Y_2O_3 by single-crystal neutron diffraction[13] and on ZrO_2 20 mol % Y_2O_3 by EXAFS and XANES[22] also propose cation displacements along $[111]_f$. More recently, results of single-crystal neutron diffraction on $Zr_{0.96}Y_{0.04}O_{1.64}N_{0.223}$ suggest shifts of the ions surrounding anion vacancies.[23]

The material of composition 10 mol % Y_2O_3 presents similar SAED patterns and HRTEM images to those of the

(14) Rao, J. C.; Zhou, Y.; Li, D. X. *J. Mater. Res* **2001**, *16* (6), 1806.
(15) Kondoh, J.; Kikuchi, S.; Tomii, Y.; Ito, Y. *J. Electrochem. Soc.* **1998**, *145*, 1536.
(16) Kondoh, J.; Kikuchi, S.; Tomii, Y.; Ito, Y. *Physica B* **1999**, *262*, 177.
(17) Lanteri, V.; Heuer, A. H.; Mitchell, T. F. *Adv. Ceram.* **1984**, *12*, 11.
(18) Suzuki, S.; Tanaka, M.; Ishigame, M. *Jpn. J. Appl. Phys.* **1985**, *24* (4), 401.
(19) McClellan, K. J.; Xiao, S. Q.; Lagerlof, K. P. D.; Heuer, A. H. *Philos. Mag., A* **1994**, *70* (1), 185.
(20) Heuer, A. H.; Chaim, R.; Lanteri, V. *Adv. Ceram.* **1988**, *24*, 3.
(21) Ishizawa, N.; Matsushima, Y.; Hayashi, M.; Ueki, M. *Acta Crystallogr., Sect. B* **1999**, *55*, 726.
(22) Li, P.; Chen, I. W.; Penner-Hahn, J. E. *Phys. Rev. B* **1993**, *48* (14), 10074.
(23) Kaiser-Bischoff, I.; Boysen, H.; Frey, F.; Hoffmann, J. U.; Hohlwein, D.; Lerch, M. *J. Appl. Cryst.* **2005**, *38*, 139.

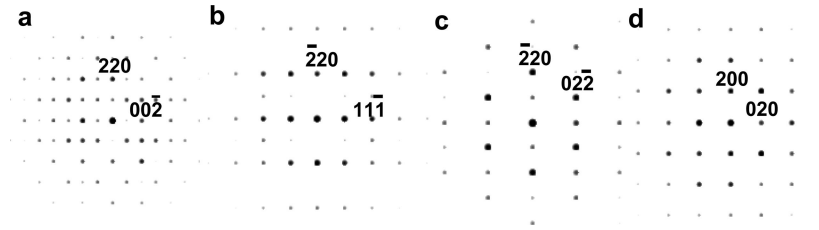

Figure 5. Calculated SAED patterns for cubic 8YSZ with 0.1 Å of cation displacements along the $[101]_f$ corresponding to the (a) $[\bar{1}10]_f$, (b) $[\bar{1}1\bar{2}]_f$, (c) $[\bar{1}1\bar{1}]_f$, and (d) $[001]_f$ zone axes.

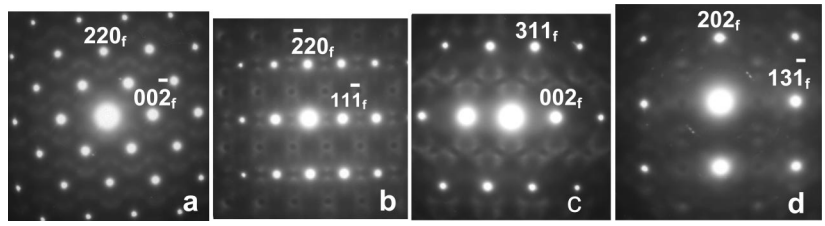

Figure 6. SAED patterns of 21YSZ along the (a) $[\bar{1}10]_f$, (b) $[\bar{1}1\bar{2}]_f$, (c) $[1\bar{3}0]_f$, and (d) $[323]_f$ zone axes.

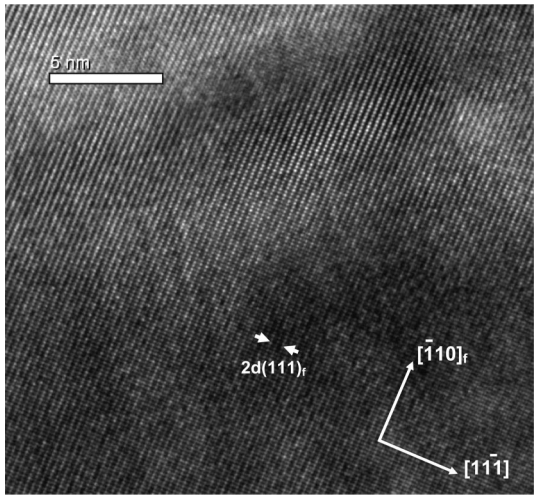

Figure 7. HRTEM image of 21YSZ corresponding to the $[\bar{1}1\bar{2}]_f$ zone axis.

8YSZ; however, the superlattice reflections do not appear in the SAED patterns of the materials of 14, 21, and 32 mol % Y_2O_3.

Figure 6 shows different SAED patterns of 21YSZ. In addition to the Bragg reflections of the fluorite type structure, diffuse scattering, characteristic of a modulation of the crystal structure, is the main feature of these patterns. Diffuse rings at $G_F \pm 1/2(\bar{1}3\bar{1})^*$ positions and two very weak reflections at both sides of $G_F \pm 1/2(11\bar{1})^*$, which are part of a diffuse ring, are observed. Therefore, diffuse scattering is located in the form of rings centred at $G_F \pm 1/2(11\bar{1})^*$ and equivalent positions with the normal axis parallel to the $[111]_f$ direction (see Figure 2 in ref24). We ascribe this diffuse scattering distribution to partial or short range ordering of the oxygen vacancies like in the pyrochlore structure,[24,25] which can be described as a superstructure of the fluorite type because of ordering of the anion vacancies forming zigzag chains along the $[110]_f$ direction (see Figure 3 in ref24). Long-range ordering of the vacancies would cause superlattice reflections at $G_F \pm 1/2(111)^*$ instead of diffuse scattering at these positions. Although cation ordering can also occur within the pyrochlore type structure, ordering between Zr and Y cannot be distinguished by electron diffraction. In addition to the short-range ordering of vacancies, atomic displacements of the ions close to the vacancies must occur, as indicated by the presence of "dark lines" intersecting the diffuse rings and the asymmetry in the intensity of both sides of the ring across the dark lines[8−10] (see the rings far from the origin in the SAED patterns of the $[\bar{1}1\bar{2}]_f$ zone axis). In addition to this, the patterns also show diffuse scattering at $G_F \pm (1/4 + \partial)(220)^*$ positions. In fact, the patterns present a continuous wave type of diffuse distribution which runs through $G_F \pm 1/2(11\bar{1})^*$ and $G_F \pm (1/4 + \partial)(220)^*$ sites. Reflections at $G_F \pm 1/4(220)^*$ are related to the C-type structure of Ln_2O_3 oxides (Ln = rare earth element), which can also be described as a superstructure of the fluorite by ordering of anion vacancies (see Figure 9 in ref24). Therefore, these patterns indicate a partial or short-range ordering of anion vacancies intermediate between the pyrochlore type and the C-type fluorite-based structures, similar to that we have previously reported in some phases of the $ZrO_2-Y_2O_3-Nb_2O_5$ system.[24,25]

Diffuse scattering has previously been observed in the SAED patterns of YSZs quenched from high temperatures for composition ranging from 14 to 32 mol% Y_2O_3.[7,15,16,18,26−28] In the current work, specific crystallographic models are proposed to explain these diffuse features based upon partial or short-range ordering of anion vacancies intermediate between the pyrochlore type and the C-type fluorite-based structures. On the contrary, Suzuki et al. proposed a modulation of the fluorite structure attributed to displacements of the oxygen ions.[18,26] Kondoh et al.[15,16] and Butz et al.[7] relate the diffuse scattering to short range ordering of

(24) García-Martín, S.; Alario-Franco, M. A.; Fagg, D. P.; Feighery, A. J.; Irvine, J. T. S. *Chem. Mater.* **2000**, *12*, 1729.
(25) García-Martín, S.; Alario-Franco, M. A.; Fagg, D. P.; Irvine, J. T. S. *J. Mater. Chem.* **2005**, *15*, 1903.
(26) Suzuki, S.; Tanaka, M.; Ishigame, M. *J. Phys. C: Solid State Physics* **1987**, *20*, 2963.
(27) Gallardo-López, A.; Martínez-Fernández, J.; Domínguez-Rodríguez, A.; Ernst, F. *Philos. Mag., A* **2001**, *81* (7), 1675.
(28) Gallardo-López, A.; Martínez-Fernández, J.; Domínguez-Rodríguez, A. *J. Eur. Ceram. Soc.* **2002**, *22*, 2821.

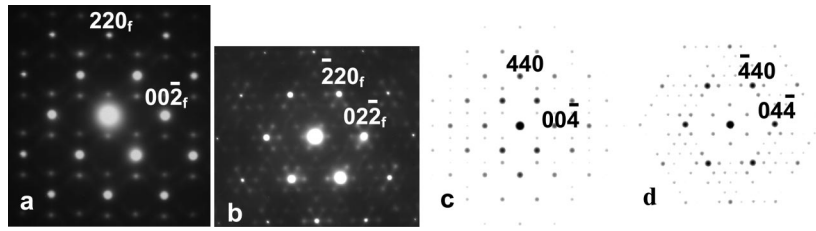

Figure 8. SAED patterns of 37YSZ along the (a) $[\bar{1}10]_f$ and (b) $[\bar{1}1\bar{1}]_f$ zone axes. Calculated SAED patterns of C-type Y_2O_3 along the (c) $[\bar{1}10]$ and (d) $[\bar{1}1\bar{1}]$ zone axes.

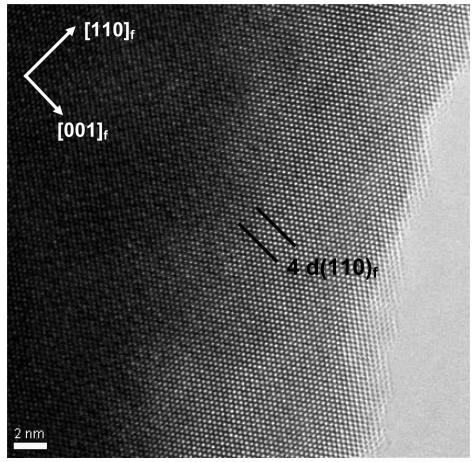

Figure 9. HRTEM image of 37YSZ corresponding to the $[1\bar{1}0]_f$ zone axis.

the oxygen vacancies although they do not propose any model of vacancies association and A. Gallardo-López et al.[27,28] explain their results by a model of microdomains of the δ-$Zr_3Y_4O_{12}$ phase oriented along different directions.

Microdomain formations of this type should be detected by TEM. Fig. 7 shows the HRTEM image along the $[\bar{1}1\bar{2}]_f$ zone axis of 21YSZ. The image is characteristic of an average fluorite structure and does not reveal two-phase formation but very weak contrast differences in some thick parts of the crystal, which indicate a periodicity of twice $d\{111\}_f$, as would correspond to a pyrochlore-type short-range ordering of the oxygen vacancies. Besides, the absence of the δ-$Zr_3Y_4O_{12}$ phase in the current work is consistent with quenching from 1500°C, a temperature above the congruent point for disorder of the compound $Zr_3Y_4O_{12}$.[29]

The modulation of the crystal structure evolves to C-type ordering of the anion vacancies with increasing yttrium concentration. Images a and b in Figure 8 show two SAED patterns of 37YSZ. Superlattice reflections related to the C-type structure of the Ln_2O_3 oxides (Ln = lanthanide element) are seen, as can be concluded from the calculated patterns of the C-type Y_2O_3 (patterns c and d in Figure 8). $G_F \pm (1/4)(220)^*$ reflections are not allowed by the $Ia\bar{3}$ space group but can be due to dynamic effects, the $G_F \pm (1/4)(22\bar{4})^*$ position being the origin of the secondary diffraction.

The HRTEM images of this sample are also characteristic of a single phase. Figure 9 shows the image corresponding to the $[\bar{1}10]_f$ zone axis, which reveals an average fluorite-type structure and presents faint dark fringes parallel to $[001]_f$ separated by four times $d(110)_f$ in some regions of the crystal.

Conclusions

We have studied different high-temperature-quenched oxides of the cubic region of the phase diagram of the $ZrO_2-Y_2O_3$ system by SAED and HRTEM. In all the SAED patterns, superlattice reflections of the cubic fluorite-type structure and/or diffuse scattering appear, which indicate a modulation of the fluorite structure.

The SAED patterns of 8YSZ and 10YSZ are characteristic of a t or t′ phase with formation of three kinds of microdomains with their *c* axes oriented along three mutually perpendicular directions. However, some features of the HRTEM images of this oxide can be explained by taking into account cation displacements from either the cubic fluorite-type structure or from its tetragonal polymorph along several possible directions. Calculated SAED patterns of all these distorted models are consistent with the experimental patterns.

At compositions of 12 mol % Y_2O_3 and higher, these tetragonal domains are not apparent. This indicates that the driver for short range order at the low Y_2O_3 concentrations in quenched cubic samples is the same as that for phase transformation for equilibrated samples with slightly lower or similar Y_2O_3 concentrations. The tetragonal distortion arises because of the small size of the Zr ionic radius favouring lower oxide coordination than eightfold, mitigating against an ideal cubic fluorite structure. Short-range anion-vacancy association does seem to occur for 12 mol % Y_2O_3 and higher. The diffuse scattering observed in the SAED patterns is characteristic of a partial or short-range ordering of the anion vacancies intermediate between the pyrochlore-type and the rear earth oxide C-type structures.

The modulation of the crystal structure evolves in such a way that the SAED patterns of compositions down to 37 mol % Y_2O_3 are consistent with C-type ordering.

HRTEM images of all these oxides show single-phase compounds.

These results explain the decreasing ionic conductivity of YSZ's with dopant concentrations higher than about 10 mol % Y_2O_3. Up to this composition, anion vacancies are distributed at random, although distortion of the cubic structure is observed. However, short-range anion-vacancy association arises at higher Y_2O_3 contents, which impacts

(29) Du, Y.; Jin, Z.; Huang, P. *J. Am. Ceram. Soc.* **1991**, *74* (7), 1569.

the anion transport. We have proposed some models for this vacancy association based on the pyrochlore- and/or C-type structures.

Acknowledgment. S.G.-M. thanks the Spanish MEC for funding the projects MAT2004-03070-C05-05 and MAT2007-64486-C07-04 and CAM for the project MATERYENER S 505/PPQ/0358. The authors also thank the Microscopy Centre Luis Bru from U.C.M. for technical assistance. J.I. thanks EPSRC for Senior Fellowship, Platform and Carbon vision support.

CM801818Y